ChemComm

Accepted Manuscript

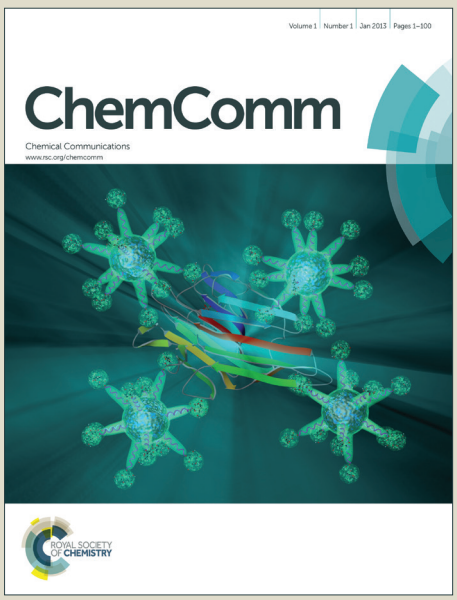

ROYAL SOCIETY OF CHEMISTRY

www.rsc.org/chemcomm

Journal Name
Cite this: DOI: 10.1039/c0xx00000x
www.rsc.org/xxxxxx
ChemComm
Dynamic Article Links ►
ARTICLE TYPE

Synthesis and Characterization of Functional Multicomponent Nanosized Gallium Chelated Gold Crystals

Ajit Zambre,[a‡] Francisco Silva,[b‡] Anandhi Upendran,[c] Zahra Afrasiabi,[d] Yan Xin,[e] António Paulo,[b] and Raghuraman Kannan[a,f,g]*

Received (in XXX, XXX) Xth XXXXXXXXX 20XX, Accepted Xth XXXXXXXXX 20XX
DOI: 10.1039/b000000x

In this communication, we describe a novel synthetic method for fabricating multicomponent gold nanoparticles containing both gallium ions and biomolecules on the surface. Detailed compositional analysis, using STEM-HAADF and EELS spectroscopy, confirmed the crystalline nature of gold and chelation of gallium ions. The biomolecule presence was validated by conventional ELISA.

Design and synthesis of multicomponent nanomaterials (MCNs) have attracted significant research interests owing to their promising applications in the field of medicine.[1,2] MCNs combine physical and biological properties of multiple materials within a single nanoconstruct. Such combinations provide unique opportunities in simultaneous detection and treatment of various human diseases.[1] On the other hand, design of multiple components within a single platform poses significant challenges in synthesis and characterization of these nanomaterials.[3] Nevertheless, it is vital to ensure that each nanoparticle comprises materials of desired composition and the inherent properties are retained to obtain the expected clinical benefits.[4] Indeed, we focused our research in addressing important challenges, including synthesis, precise atomic level identification, quantification, and characterization, in the fabrication of gold nanoparticle (AuNP) based MCNs. Specifically, in this communication, we report the synthesis and detailed characterization of MCNs of formula [AuNP(Ga)(HRP)]; (HRP = Horseradish peroxidase). The rationale for choosing these components in our MCN design is as follows: (i) AuNPs possess significant advantages including rich-surface chemistry, non-toxic behavior, and non-immunogenic characteristics;[4,5] (ii) Ga-67 and Ga-68 are gamma and positron emitting isotopes respectively, and are widely used in molecular imaging;[6] and (iii) HRP serves as a model biomolecule and its presence can be confirmed by conventional ELISA techniques.[7]

In our MCN design, we used AuNPs conjugated with an amino-carboxylate ligand (diethylene triamine pentaacetic acid, DTPA) on the surface via dithiol (DT) linkage (AuNP-DTDTPA).[8-10] Pioneering efforts by Roux and coworkers have shown that AuNP-DTDTPA is an excellent platform for conjugating with Gd, In, or ^{99m}Tc, and these elements have excellent molecular imaging capabilities.[8-10] Dithiolated DTPA (DTDTPA) has several unique advantages such as smaller bite size, presence of both soft N-donor and hard O-donor ligands.[8,9] Unlike other N, O-ligands, DTPA forms kinetically inert and thermodynamically stable metal complexes under normal laboratory conditions. DTPA based metal chelates have shown excellent *in vivo* stability.[10,11] Such characteristic features of DTPA bring numerous potential clinical benefits for *in vivo* imaging.[11] For these reasons, [AuNP(DTDTPA)] (**1**) conjugate is emerging as a promising platform for developing biologically useful MCNs. As part of our ongoing studies in the design and development of gold nanoparticles,[12,13] we report (i) synthesis of [AuNP(DTDTPA)(Ga)] (**2**), (**Scheme 1**); (ii) characterization of **2** using advanced Scanning Transmission Electron Microscopy (STEM) techniques; (iii) detailed *in vitro* stability and cytotoxicity studies of **2**; and (iv) synthesis and characterization of [AuNP(DTDTPA)(Ga)(HRP)] (**3**).

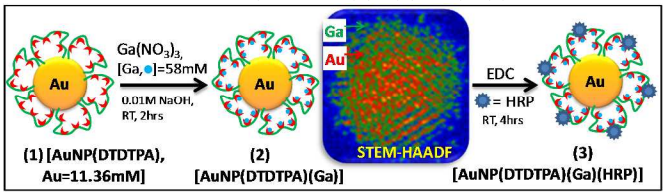

Scheme 1. Synthesis of **2** and **3**.

We began our investigation by understanding the structural and physicochemical properties of **1**. Specifically, we were interested in understanding the integrity of multi-layered carboxylate structure of **1** among various pH and dilutions (see ESI). The layered carboxylate structure is crucial for attachment of different components. Our intent was to utilize carboxylate layers for both metal and biomolecule conjugation. Our detailed studies confirmed that the multilayered carboxylate architecture is fairly stable over a wide range of pH (6 to 13) and at different concentrations (30 µg/ml to 5 mg/ml).

[AuNP(DTDTPA)(Ga)] (**2**) was synthesized by treating **1** with $Ga(NO_3)_3$ at pH 8.0 (**Scheme 1**). The optimized ratio of Au:Ga is 1:5. Complex **2** exhibits a core size of ~3-5 nm, hydrodynamic size of 88 nm and a -55 mV zeta potential. In order to investigate the maximum concentration of gallium that can be incorporated within the nanoconstruct (**1**) we performed serial titrations of **1** with Ga^{3+} and evaluated the resultant conjugate using both Ga-71 NMR spectroscopy and ICP-OES analysis (ESI-Figure 1). The NMR active ^{71}Ga is used as a probe to determine the concentration of chelated Ga. NMR of different concentrations of $Ga(NO_3)_3$ were recorded in D_2O (ESI–Figure 2). A standard curve using concentrations of non-chelated Ga vs. peak integration values were plotted. Using the plot, we determined that 11 mM of Au can irreversibly chelate up to 58 mM of Ga. That indicates any gallium added beyond this concentration would not be chelated with AuNP-DTDTPA. The NMR results were validated by performing additional experiments using ICP-OES. In this experiment, we monitored Au/Ga ratios of the resultant conjugates after treatment of 11 mM of **1** (Au) with different amounts of Ga^{3+}. Au/Ga ratio

becomes a constant after addition of 58 mM of Ga^{3+}. By these experiments, we have demonstrated the exact concentration of Ga that can be irreversibly chelated to **1**. The smaller core size of **2** made the characterization quite challenging. We utilized multiple analytical tools (UV-Vis, TEM, DLS, XPS, EDX, HAADF, and EELS; see supporting information for all characterization data) to obtain structural details of **2**. Conventional techniques such as UV-Vis and TEM confirmed that the crystallinity of gold core **1** is retained after chelation with Ga. As the gold core size is less than 5 nm, the plasmon resonance (λ_{max}) showed a small hump at 520 nm before and after complexation.

Nanoconstruct **2** has been characterized by STEM in a probe corrected JEM-ARM200cF at 200kV. The STEM high angle annular dark field (HAADF) Z-contrast images show the Au atoms in white contrasts in **Figure 1**. From a lower magnification image (**Figure 1a**), the AuNP size distribution can be obtained accurately since the contrast is reflecting the real size of the particles without any diffraction interference contrast. The AuNP shows three size categories, with the biggest diameter of 3.77 ± 0.25 nm, the medium ones of 2.43 ± 0.27 nm, and the smallest ones of 1.15 ± 0.13 nm. The atomic structure of a typical crystalline AuNP is shown in **Figure 1b** with a higher magnification. The nanoparticle denoted as **A** in **Figure 1b** is projected along [110] direction exhibiting the 5-fold twinning structure. The smaller particle **B** does not show crystallinity, only forming a cluster of Au atoms. It is believed that the biggest AuNP particles were aggregated due to the irritation of the electron beam. The white speckles on the dark background in the image are the scattered individual Au atoms. Some of the smallest clusters of AuNP are probably formed from these scattered Au atoms under the beam. This formation may be due to incident electron beam or beam induced heating (ESI-Figure 15). Similar effects have been observed in smaller gold clusters and reported elsewhere.[14] Interestingly, we noted the movement of **2** under electron beam (Video clip uploaded as ESI). The lattice parameter of the AuNP has been deduced from the images of particles (similar to particle **A**), and it is measured to be 0.418 nm. It is larger than the Au bulk lattice parameter (0.408 nm). Since Ga atoms are much lighter than the Au atoms, where the HAADF image contrast is proportional to the atomic number $Z^{1.7}$, it is hard to discern the contrast of the Ga atoms on the amorphous carbon background in the HAADF image without quantitative experimental data. Therefore, the electron energy loss spectroscopy (EELS) and Spectrum Imaging (SI) technique were used to detect the presence of the Ga in the samples as shown in **Figure 1c** to **1e**. **Figure 1c** is the HAADF view of the sample and the green box is the scanning region for SI, where core loss EELS spectra were collected on each pixel location of the scanned region. **Figure 1d** shows the EELS spectrum from a point between the two AuNP particles, and unmistakably showing the presence of Ga (L2, 3 due to core loss edge at 1115 eV). **Figure 1e** presented the spectrum obtained from the top of the right AuNP. In this spectrum, it clearly shows the presence of both Ga L2,3 (peak at 1115) and Au M4,5 (peak at 2206 eV), confirming the presence of Ga on the top of AuNP. In all, the SI data confirmed that Ga is present and surrounding AuNP.

It is expected that the Ga^{3+} will effectively complex with carboxylate anions and amines closer to the surface of gold. AuNP-DTDTPA-Ga structure was further analysed by using XPS measurements. Of particular interest to the present study is the binding of gallium to the surface ligand, DTDTPA. It is worth to note here that surface bound DTDTPA is rich in disulfides, secondary amines, and carboxylates. Even though the metallic alloy of Ga with Au is known at 400°C, it is unexpected in the present scenario.[15,16] It is possible that Ga^{3+} can bind with thiol; however, thiols are present predominantly as disulfides in the parent nanoconstruct.[8,9] Such a binding would require oxidative addition of Ga^{3+} across disulfide bonds, which is not feasible based on the chemistry of gallium. However, N and O atoms present in the ligand is geometrically positioned to chelate with Ga. In the conjugate **2**, the N(1S) levels showed a peak at 398.8eV (ESI-Figure 16). The literature studies have demonstrated the N/S levels are not sensitive to these binding events.[14]

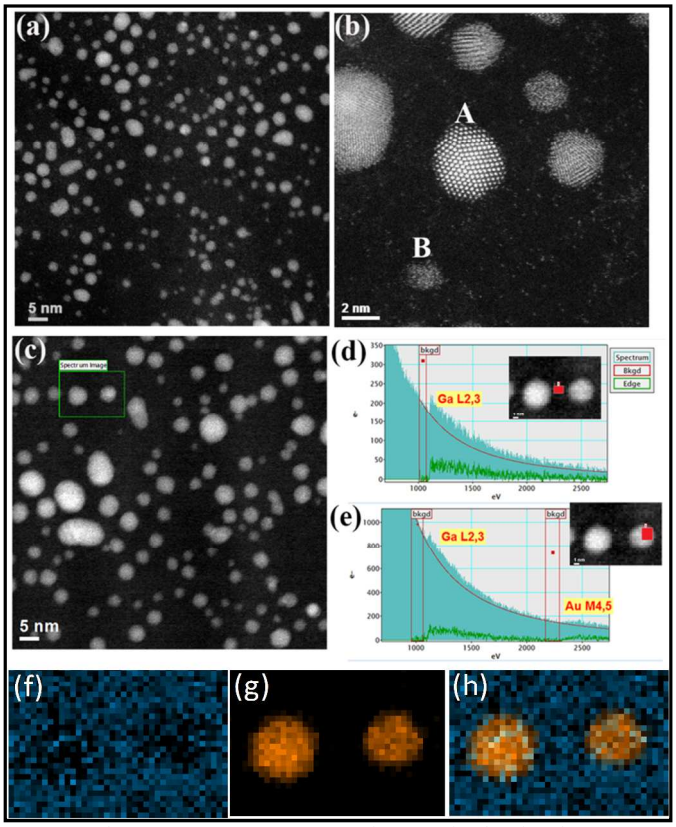

Figure 1. The STEM–HAADF Z-contrast images of **2** showing the Au atoms in white contrasts. (a) Lower magnification image; (b) The atomic structures of a typical crystalline AuNP shown under high magnification; (c) HAADF view of the sample with a scanning region shown by green outline; (d) EELS spectrum from a point between the two Au particles; (e) Spectrum obtained from the top of the right AuNP showing presence of Ga; Elemental mapping images of **2** showing (f) Gallium emission; (g) Gold emission; and (h) Composite emission of Au and Ga distributions for two nanoparticles.

Having established the synthesis and characterization of [AuNP(DTDTPA)Ga] (**2**) conjugate, we focused our attention to explore further utilization of carboxylate ligands on **2** for conjugating with biomolecules. As a proof-of-concept, we conjugated HRP to carboxylates on **2**. Presence of HRP was detected by conventional ELISA technique.[7] We utilized two different conjugates of **2**, with varying amounts of Ga present in nanoconjugate, namely, conjugates obtained after treatment of **1** with 29 mM of Ga and another one with the saturating amount of 58 mM. Low concentration of gallium (less than required for complete chelation) was used deliberately to increase the number of free carboxylates while a very high amount (more than required for complete chelation) was used to utilize all possible carboxylates present in the nanoconstruct. The absorbance of conjugated HRP was plotted against concentration of nanoconstruct (**2**) to relate the

binding capabilities. **Figure 2** shows absorbance of conjugated HRP with serial 10 fold dilutions of **2**. It was obvious to note that the absorbance increases with increasing concentration of **2** as the HRP holding capability of **2** increases. On the other hand, chelates with varying concentrations of Ga (29 mM and 58 mM) did not show any difference in conjugation with HRP. (**Figure 2** *inset*) This data suggests that HRP conjugation with **2** is independent of amount of chelated Ga.

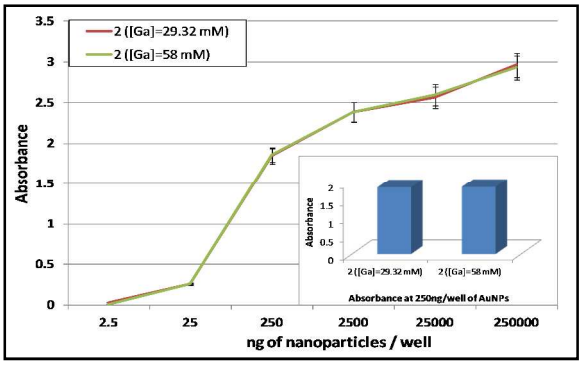

Figure 2. ELISA binding plot of **2** with two concentrations (29.32 and 58.0 mM) of $Ga(NO_3)_3$ reacted with **1** for the determination of peroxidase activity; and *inset* shows carboxylate conjugation efficiency of **2** with HRP by ELISA.

Based on our analytical and microscopy data, it is fair to assume that HRP is conjugated with sterically less-crowded carboxylates that are available after gallium chelation on the nanoparticle. This could be due to the fact that surface attached DTDTPA ligand would possibly exhibit two kind of carboxylates on the surface; the first kind would be a part of compact ligand structure that are ideally required for chelation of gallium and the second kind would be carboxylates that are not conformationally favourable to form a thermodynamically stable metal chelate. The second kind of carboxylates is available for biomolecule conjugation. The possibility of interaction of gallium atoms with these conformationally unfavourable carboxylates is minimal. Due to this binding preference of gallium and HRP, we reason that HRP conjugation efficiency remains the same for both low (29 mM) and high (58 mM) gallium chelated AuNP.

The cytotoxicity of **1** and **2** was studied on human prostate cancer (PC-3) cells under *in vitro* conditions using a colorimetric cell-viability (MTT) assay (ESI-Figure 7). The results demonstrate that nanoconstructs **1** and **2** do not show cytotoxicity up to 40 µg/mL concentrations. Nevertheless, the cell viability was slightly lesser for **2** than **1** for the period of 24 h post treatment. It is worth to mention here that AuNPs are non-toxic.[17] In addition, our studies showed that nanoconstruct **1**, containing DTDTPA ligand coating on the surface of AuNPs, is non-toxic. Therefore, the minimal toxicity exhibited by **2** may be attributed to conjugated gallium. The lack of any noticeable toxicity of **1** and **2** thereby provide new opportunities for utilizing these conjugates for biomedical imaging.

Conclusions

We demonstrated that **1** can serve as an ideal platform for synthesizing MCNs containing metal atoms and biomolecules. The presence of all three components, Au, Ga, and biomolecule in single MCN has been synthesized and characterized using sophisticated analytical techniques. Such MCNs with radiolabeled metals can serve as a unique scaffold for conjugation of diverse biomolecules for specific targeting with molecular imaging capability.

R.K. acknowledges the Michael J. and Sharon R. Bukstein Faculty Professorship endowment on Cancer Research for financial support. Authors also acknowledge funding from NIH-SBIR Phase II contract, USDA –NIFA grant, Coulter Translational Program Bridge award, MU iCATS Faculty Innovator Award, Fast Track Economic Development Award, and Mizzou Advantage award. The EELS work was carried out at Florida State University (FSU) and the facility is funded and supported by the FSU Research Foundation, National High Magnetic Field Laboratory (NSF-DMR-0654118) and the State of Florida. Authors acknowledge Dr. Wen Ritts, Electron Microscopy Core Facility at University of Missouri-Columbia.

Notes and references

[a]Departments of Radiology, [c]Physics and [f]Bioengineering, [g]International Center for Nano/Micro Systems and Nanotechnology, University of Missouri-Columbia, Columbia, Missouri-65212. USA; Tel: 0015738825676; E-mail: kannanr@health.missouri.edu
[b]Centro de Ciências e Tecnologias Nucleares, Instituto Superior Técnico, Estrada Nacional 10 (Km 139,7), 2695-066 Bobadela LRS, Portugal.
[d]Department of Life and Physical Sciences, Lincoln University, Jefferson City, Missouri 65101, USA
[e]National High Magnetic Field Laboratory, Florida State University, Tallahassee, FL 32310, USA
[‡]These authors contributed equally.

1. Giljohann DA, Seferos DS, Daniel WL, Massich MD, Patel PC, Mirkin CA. Gold nanoparticles for biology and medicine. *Angew Chem Int Ed Engl.* Apr 26 2010;49(19):3280-3294.
2. Ferrari M. Cancer nanotechnology: opportunities and challenges. *Nat Rev Cancer.* Mar 2005;5(3):161-171.
3. Wang D, Li Y. Bimetallic nanocrystals: liquid-phase synthesis and catalytic applications. *Adv Mater.* Mar 4 2011;23(9):1044-1060.
4. Desai N. Challenges in development of nanoparticle-based therapeutics. *AAPS J.* Jun 2012;14(2):282-295.
5. Eifler AC, Thaxton CS. Nanoparticle therapeutics: FDA approval, clinical trials, regulatory pathways, and case study. *Methods Mol Biol.* 2011;726:325-338.
6. Chitambar CR. Medical applications and toxicities of gallium compounds. *Int J Environ Res Public Health.* May 2010;7(5):2337-2361.
7. Samara P, Kalbacher H, Ioannou K, et al. Development of an ELISA for the quantification of the C-terminal decapeptide prothymosin alpha(100-109) in sera of mice infected with bacteria. *J Immunol Methods.* Sep 30 2013;395(1-2):54-62.
8. Alric C, Taleb J, Le Duc G, et al. Gadolinium chelate coated gold nanoparticles as contrast agents for both X-ray computed tomography and magnetic resonance imaging. *J Am Chem Soc.* May 7 2008;130(18):5908-5915.
9. Debouttière P-J, Roux, S., Vocanson, F., Billotey, C., Beuf, O., Favre-Réguillon, A., Lin, Y., Pellet-Rostaing, S., Lamartine, R., Perriat, P. and Tillement, O. Design of Gold Nanoparticles for Magnetic Resonance Imaging. *Adv Funct Mat.* 2006;16:2330-2339.
10. Alric C, Miladi I, Kryza D, et al. The biodistribution of gold nanoparticles designed for renal clearance. *Nanoscale.* Jul 7 2013;5(13):5930-5939.
11. Moi MK, DeNardo SJ, Meares CF. Stable bifunctional chelates of metals used in radiotherapy. *Cancer Res.* Feb 1 1990;50(3 Suppl):789s-793s.
12. Chanda N, Kattumuri V, Shukla R, et al. Bombesin functionalized gold nanoparticles show in vitro and in vivo cancer receptor specificity. *PNAS USA.* May 11 2010;107(19):8760-8765.
13. Chanda N, Shukla R, Katti KV, Kannan R. Gastrin releasing protein receptor specific gold nanorods: breast and prostate tumor avid nanovectors for molecular imaging. *Nano Lett.* May 2009;9(5):1798-1805.
14. Wang ZW, Palmer RE. Mass spectrometry and dynamics of gold adatoms observed on the surface of size-selected Au nanoclusters. *Nano Lett.* Jan 11 2012;12(1):91-95.
15. Yazdanpanah MM HS, Cohn RW. Gallium-driven assembly of gold nanowire networks. *Applied Phys Lett.*. 2004;85(9):1592-1594.
16. Weizer VG FN. The interaction of gold with gallium arsenide. *J Applied Phy.* 1988;64(9):4618-4623.
17. E. E. Connor, J. Mwamuka, A. Gole, C. J. Murphy and M. D. Wyatt, *Small*, 2005, **1**, 325-327.